Impact of the Manaus urban plume on trace gas mixing ratios near the surface in the Amazon Basin: Implications for the NO-NO_2-O_3 photostationary state and peroxy radical levels

Ivonne Trebs,[1] Olga L. Mayol-Bracero,[1,2] Theotonio Pauliquevis,[3,4] Uwe Kuhn,[1,5] Rolf Sander,[6] Laurens Ganzeveld,[7] Franz X. Meixner,[1] Jürgen Kesselmeier,[1] Paulo Artaxo,[3] and Meinrat O. Andreae[1]

Received 9 June 2011; revised 13 January 2012; accepted 13 January 2012; published 13 March 2012.

[1] We measured the mixing ratios of NO, NO_2, O_3, and volatile organic carbon as well as the aerosol light-scattering coefficient on a boat platform cruising on rivers downwind of the city of Manaus (Amazonas State, Brazil) in July 2001 (Large-Scale Biosphere-Atmosphere Experiment in Amazonia-Cooperative LBA Airborne Regional Experiment-2001). The dispersion and impact of the Manaus plume was investigated by a combined analysis of ground-based (boat platform) and airborne trace gas and aerosol measurements as well as by meteorological measurements complemented by dispersion calculations (Hybrid Single-Particle Lagrangian Integrated Trajectory model). For the cases with the least anthropogenic influence (including a location in a so far unexplored region ~150 km west of Manaus on the Rio Manacapuru), the aerosol scattering coefficient, σ_s, was below 11 Mm^{-1}, NO_x mixing ratios remained below 0.6 ppb, daytime O_3 mixing ratios were mostly below 20 ppb and maximal isoprene mixing ratios were about 3 ppb in the afternoon. The photostationary state (PSS) was not established for these cases, as indicated by values of the Leighton ratio, **Φ**, well above unity. Due to the influence of river breeze systems and other thermally driven mesoscale circulations, a change of the synoptic wind direction from east-northeast to south-southeast in the afternoon often caused a substantial increase of σ_s and trace gas mixing ratios (about threefold for σ_s, fivefold for NO_x, and twofold for O_3), which was associated with the arrival of the Manaus pollution plume at the boat location. The ratio **Φ** reached unity within its uncertainty range at NO_x mixing ratios of about 3 ppb, indicating "steady-state" conditions in cases when radiation variations, dry deposition, emissions, and reactions mostly involving peroxy radicals (XO_2) played a minor role. The median midday/afternoon XO_2 mixing ratios estimated using the PSS method range from 90 to 120 parts per trillion (ppt) for the remote cases (σ_s < 11 Mm^{-1} and NO_x < 0.6 ppb), while for the polluted cases our estimates are 15 to 60 ppt. These values are within the range of XO_2 estimated by an atmospheric chemistry box model (Chemistry As A Box model Application-Module Efficiently Calculating the Chemistry of the Atmosphere (CAABA/MECCA)-3.0).

Citation: Trebs, I., O. L. Mayol-Bracero, T. Pauliquevis, U. Kuhn, R. Sander, L. Ganzeveld, F. X. Meixner, J. Kesselmeier, P. Artaxo, and M. O. Andreae (2012), Impact of the Manaus urban plume on trace gas mixing ratios near the surface in the Amazon Basin: Implications for the NO-NO_2-O_3 photostationary state and peroxy radical levels, *J. Geophys. Res.*, *117*, D05307, doi:10.1029/2011JD016386.

[1]Biogeochemistry Department, Max Planck Institute for Chemistry, Mainz, Germany.
[2]Now at Institute for Tropical Ecosystem Studies, University of Puerto Rico, Río Piedras, Puerto Rico.
[3]Instituto de Física, Universidade de São Paulo, São Paulo, Brazil.
[4]Now at Departamento de Ciências Exatas e da Terra, Universidade Federal de São Paulo, Diadema, Brazil.
[5]Now at Juelich Research Center, Institute of Energy and Climate Research: Troposphere, Juelich, Germany.
[6]Air Chemistry Department, Max Planck Institute for Chemistry, Mainz, Germany.
[7]Department of Environmental Sciences, Wageningen University and Research Centre, Wageningen, Netherlands.

0148-0227/12/2011JD016386

1. Introduction

[2] The chemistry of nitrogen oxides (NO_x, the sum of nitrogen monoxide, NO, and nitrogen dioxide, NO_2) within the planetary boundary layer was studied in detail during the last decades in many regions of the globe. It is well known that NO_x acts as a key catalyst in the formation of tropospheric ozone (O_3) [*Crutzen and Lelieveld*, 2001]. In the absence of competing reactions, a dynamic equilibrium between NO, NO_2, and O_3 (also called photostationary state (PSS)) may be established during daytime in the troposphere:

$$\text{(R1)} \qquad NO_2 + h\nu\ (\lambda < 420\ \text{nm}) \rightarrow NO + O(^3P)$$

$$\text{(R2)} \qquad O(^3P) + O_2 + M \rightarrow O_3 + M$$

$$\text{(R3)} \qquad NO + O_3 \rightarrow NO_2 + O_2$$

Reaction (R2) is much faster than (R1), and therefore, reactions (R1) and (R3) determine the overall conversion rate. The PSS parameter, or Leighton ratio, Φ [*Leighton*, 1961], is defined by

$$\Phi = \frac{j(NO_2) \times [NO_2]}{k_3 \times [O_3] \times [NO]} \qquad (1)$$

where $j(NO_2)$ is the photolysis frequency of NO_2 and k_3 is the rate constant of reaction (R3) [*Atkinson et al.*, 2004]. When Φ is unity, no additional O_3 is produced and the reactions (R1) to (R3) represent a null cycle. The PSS approach is only valid under "steady-state" conditions, that is, in the absence of (1) rapid changes of light intensity and fluctuations of mixing ratios, (2) significant influence of dry deposition or fresh emissions of the involved compounds, and (3) other competing reactions.

[3] Particularly, the oxidation of NO by peroxy radicals constitutes a major net O_3 production pathway in the troposphere [e.g., *Warneck*, 2000]:

$$\text{(R4)} \qquad HO_2 + NO \rightarrow NO_2 + HO$$

$$\text{(R5)} \qquad RO_2 + NO \rightarrow NO_2 + RO$$

where R is an organic functional group (e.g., CH_3 or C_2H_5). HO_2 and RO_2 radicals (their sum hereafter referred to as XO_2) are formed from the oxidation of carbon monoxide (CO) and hydrocarbons by OH radicals. Most previous studies reported that PSS is readily established under polluted (high-NO_x) conditions [*Carpenter et al.*, 1998; *Griffin et al.*, 2007; *Parrish et al.*, 1986; *Volz-Thomas et al.*, 2003]. It was found, however, that under cleaner (low-NO_x) conditions, XO_2 may substantially perturb PSS, resulting in values of $\Phi \gg 1$ and measured NO_2 mixing ratios exceeding those predicted by equation (1) [*Bakwin et al.*, 1994; *Hauglustaine et al.*, 1996; *Ridley et al.*, 1992]. Some authors [e.g., *Mannschreck et al.*, 2004; *Volz-Thomas et al.*, 2003] suggested that other unknown oxidation processes may cause an additional conversion of NO to NO_2 leading to values of $\Phi \gg 1$. This was recently confirmed by *Hosaynali Beygi et al.* [2011] for background conditions in the remote marine boundary layer.

[4] Only few studies have investigated the NO-NO_2-O_3 triad in the Amazon Basin. These focused on the surface-atmosphere exchange fluxes of individual compounds [*Bakwin et al.*, 1990; *Ganzeveld et al.*, 2002; *Gut et al.*, 2002; *Jacob and Wofsy*, 1990; *Rummel et al.*, 2002, 2007; *Trebs et al.*, 2006], on airborne studies, or on modeling activities [*Andreae et al.*, 1988; *Crutzen et al.*, 1985; *Harriss et al.*, 1988; *Kuhn et al.*, 2010; *Lelieveld et al.*, 2008; *Torres and Buchan*, 1988]. In the Amazon, mixing ratios of the NO-NO_2-O_3 triad are substantially enhanced during the dry (biomass burning) season from June to September. However, the plume of pollutants originating from the city of Manaus (currently about 1.7 million inhabitants) is known to have an additional significant impact on atmospheric chemistry in the region west of Manaus [*Kuhn et al.*, 2010]. Furthermore, high emissions of hydrocarbons have recently been shown to sustain high radical concentrations above the Brazilian rain forest close to Manaus [*Kuhn et al.*, 2007] as well as above other tropical South American rain forest locations [cf. *Lelieveld et al.*, 2008; *Martinez et al.*, 2010], thereby affecting the cycling of NO_x and the production of O_3 in this region. The influence of anthropogenic activities and mixing conditions on atmospheric chemistry within the boundary layer in the Amazon Basin is not well understood, and no direct measurements of prevailing XO_2 radical mixing ratios have been reported so far. Likewise, an investigation of the PSS of the NO-NO_2-O_3 triad has not yet been performed in this region. A thorough understanding of the NO-NO_2-O_3 chemistry and the role of peroxy radicals is required for an assessment of future chemistry-climate interactions in tropical regions with increasing anthropogenic impact [cf. *Ganzeveld et al.*, 2010].

[5] In this paper, we investigate the PSS for the first time at unique (including very remote) measurement locations in the Amazon Basin, based on field measurements made during the Large-Scale Biosphere-Atmosphere Experiment in Amazonia-Cooperative LBA Airborne Regional Experiment (LBA-CLAIRE-2001). We used a boat platform cruising on rivers in the downwind region west of Manaus, at a distance ranging from approximately 20–150 km. We sampled clean air at remote locations as well as air masses affected by the Manaus plume, which had interacted with the rain forest and water surfaces of rivers west of Manaus. We infer XO_2 mixing ratios, and we show that the PSS approach is not valid in the low-NO_x regime of remote tropical air masses, in agreement with results obtained in other remote regions of the globe. Furthermore, our analysis provides information about the impact of anthropogenic emissions and mesoscale circulations on the pristine tropical forest photochemistry and radical formation near the surface downwind of Manaus.

2. Experimental Setup

2.1. Description of Measurement Sites and Implementation

[6] The measurements were made within the framework of LBA-CLAIRE-2001 from 10 to 27 July 2001 (wet-to-dry season transition) on a boat cruising downwind of the city of Manaus (Figure 1). Manaus had a population of about 1.2 million human inhabitants in 2001; major emission

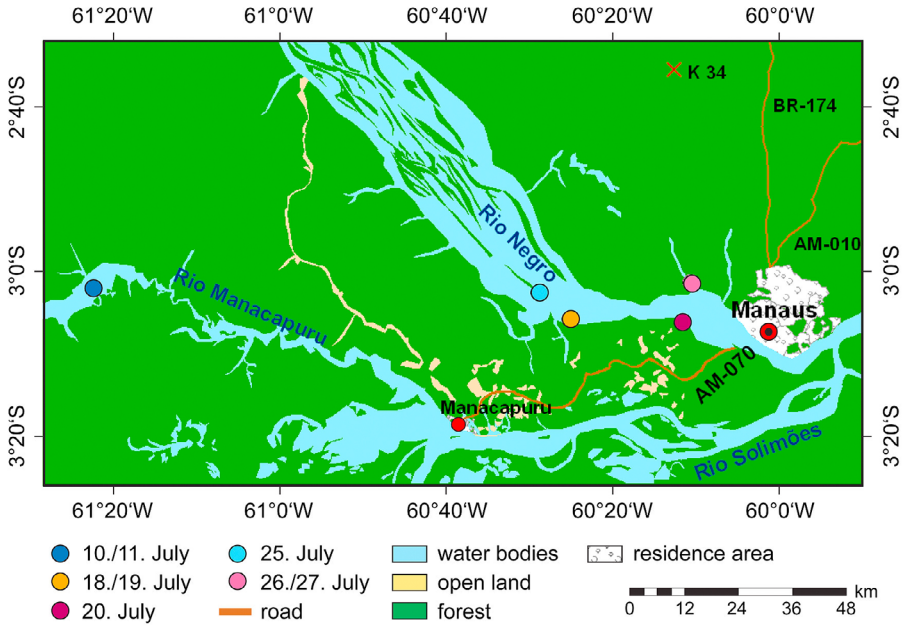

Figure 1. GIS map showing the study area and boat positions on 10–11, 18–20, and 25–27 July (LBA-CLAIRE-2001 boat experiment). The position of the boat on the different days is represented by colored circles.

sources in and around Manaus comprise thermoelectric power plants, vehicles, saw mills, charcoal kilns, brick factories, and small-scale burnings [*Kuhn et al.*, 2010].

[7] The average annual rainfall in Manaus is ~2200 mm with two marked seasons (November–May wet; June–October dry). The rain forest ecosystem characteristics of the Manaus area are described in detail by *Kuhn et al.* [2007]. The airflow is typically dominated by easterly trade winds transporting humid oceanic air masses from the Atlantic more than 1000 km over the almost undisturbed rain forest of the northeastern Amazon Basin, before reaching the urban area of Manaus.

[8] Three boat trips were performed on Rio Manacapuru (10–11 July) and on Rio Negro (18–20 and 25–27 July) (see Figure 1). During weekends the boat was located at the main station in Manacapuru (Paraiso D'Angelo: 3.297°S, 60.604°W), where instruments were maintained and calibrated. Two boat platforms were used during our experiment. The first boat was equipped with an automatic weather station and the trace gas and aerosol measuring instrumentation, while the second boat carried a diesel generator providing a power of 15 kW for operation of the instruments. A power cable was connected to an electrical manifold onboard the first boat and was kept on the water surface using floating devices. The second boat was pulled by the first boat using a 5 mm steel cable and was kept always downwind of the first boat to minimize the risk of local contamination.

2.2. Meteorological Measurements

[9] Meteorological quantities were monitored with a time resolution of 1 min on a mast at a height of 8 m above the water surface. These comprised wind speed (cup anemometer A101ML, Vector Instruments, UK), wind direction (wind vane, self-referencing, SRW1, Vector Instruments, UK), solar global irradiance (pyranometer, LI-1000, LI-COR, USA), air temperature and relative humidity (Hygromer® IN-1 and Pt100 sensor in aspirated housing, Rotronic Messgeräte GmbH, Germany), and barometric pressure (pressure analog barometer, PTA 427A, Vaisala, Finland). Rainfall was measured using a tipping rain gauge (ARG 100-EC, Campbell Scientific, UK) on the edge of the boat. The position of the boat was tracked continuously using a Global Positioning System unit (GPSHAND, ESYS, Berlin, Germany).

2.3. Trace Gas and Aerosol Measurements

[10] The inlets for trace gas and aerosol measurements were located at a level of 3 m above the water surface. The reactive trace gases, nitric oxide (NO), nitrogen dioxide (NO_2), and ozone (O_3) were measured with a time resolution of 1 min using sensitive commercially available analyzers located in the interior of the boat. NO was measured by red-filtered detection of the chemiluminescence produced during the reaction of NO and O_3 (CLD 780 TR, ECO Physics, Switzerland). Excess O_3 was continuously added in a pre-reaction chamber to account for the cross-sensitivity by other gases. NO_2 was photolytically converted to NO by exposure of the sample air to a high-pressure xenon lamp (Tecan PLC 760 photolytic converter) and then detected by the chemiluminescence analyzer. The analyzer was calibrated four times during the experiment (on 8, 13, 22, and 25 July 2001) by diluting a 5.32 ppm NO standard gas. The efficiency of the photolytic conversion of NO_2 to NO was 0.52, determined by a back titration procedure involving the reaction of O_3 with NO using a gas phase titration system (SYCOS K-GPT, ANSYCO GmbH, Germany).

[11] The climatic conditions in the Amazon Basin and the absence of air conditioning on the boat caused higher detection limits and uncertainties of the CLD 780 TR analyzer than typical for controlled conditions [cf. *Mannschreck*

et al., 2004; *Volz-Thomas et al.*, 2003]. The limit of detection (LOD) (2σ-definition, 10 min averages) for NO and NO_2 determined during the experiment by sampling synthetic (zero) air that had passed an active charcoal filter were 75 and 135 ppt, respectively. The correction applied for the systematic offset of the CLD 780 TR analyzer determined when sampling zero-air was on average 50 ppt. This value was confirmed by sampling clean air with ambient NO levels near zero during nighttime at the remote locations [cf. *Kley and McFarland*, 1980]. The precision of the chemiluminescence analyzer determined from the signal noise during the calibrations was on average 4% (2σ). The variation of the spans of the individual calibrations made on the boat platform was 20%. The influence of ambient temperature and humidity variations on the sensitivity of the chemiluminescence analyzer are about 1.3% K^{-1} and -0.27% hPa^{-1} H_2O [see *Volz-Thomas et al.*, 2003]. The temperature in the boat ranged from 25°C to 35°C. Since the calibrations were made at temperatures covering this range, the temperature effect is included in the span variation stated above. Data were not corrected for the humidity effect since it applies to both NO and NO_2 measurements and would thus not affect the value of Φ (see equation (1)).

[12] O_3 was measured with a UV absorption analyzer (Thermo Instruments, TE49C, USA), which has an accuracy of 5% and a precision of 1% at mixing ratios higher than 20 ppb. The offset of the analyzer was checked by sampling synthetic air that had passed an active charcoal filter. Grab samples for the determination of volatile organic carbon (VOC, 50 min sampling interval) were collected on fused-silica-lined stainless steel cartridges (89 mm length, 5.33 mm internal diameter; Silicosteel, Restek, USA) with two-bed graphitic carbon adsorbents (130 mg Carbograph 1, followed by 130 mg Carbograph 5; Lara s.r.l., Rome, Italy) using customized constant-flow sampler devices (courtesy Jim Greenberg, National Center for Atmospheric Research, Boulder, Colorado). The samples were analyzed off-line in the laboratory using a thermal desorption gas chromatograph with a flame ionization detector (GC-FID) as described in the study by *Kuhn et al.* [2002, 2004]. Calibration was accomplished by different gaseous standards containing isoprene, several n-alkanes, methyl vinyl ketone (MVK), and methacrolein (MACR). The detection limit was determined from the standard deviation of the blank values and was typically 30 ppt for isoprene and 10 ppt for monoterpenes. Overall uncertainties were 10% for isoprene at 1 ppb and ranged from 5% to 30% at 100 ppt for monoterpenes [cf. *Kuhn et al.*, 2007]. Additionally, aerosol light-scattering measurements were made with a single-wavelength (λ = 545 nm) nephelometer (Model M903, Radiance Research, USA) at ambient relative humidity (RH).

2.4. Companion Measurements

[13] *Kuhn et al.* [2010] reported on airborne measurements of trace gases and aerosols in the region west of Manaus, which were part of LBA-CLAIRE-2001. In this study, we use data (O_3 and aerosol number concentrations) measured during crosswind transects in the urban outflow at a longitude of ~60.41°W (~ 43 km downwind of Manaus) on 19 July (Flight 18: 10:00–14:00 LT, Flight 19: 15:45–18:00 LT). O_3 was measured with a time resolution of 10 s using the same type of instrument as on the boat platform and the aerosol number (CN) concentrations were measured at 1 Hz time resolution with a condensation particle counter (CPC; Model 3762 and 3010, TSI, USA) [cf. *Kuhn et al.*, 2010].

[14] In addition, meteorological measurements (temperature, relative humidity, wind speed, and wind direction) were made on a 52 m high walk-up scaffolding tower (K34, ca. 20 m above the forest canopy) [see *Kuhn et al.*, 2007]. The tower is located in the National Institute of Amazon Research (INPA) forest management area (Reserva Biológica do Cuieiras) in undisturbed primary forest about 60 km NNW of Manaus (2.6091°S, 60.2092°W) (see Figure 1).

2.5. Data Evaluation

[15] The 1 min time series of all measured quantities on the boat platform were combined into arithmetic averages for 10 min intervals. However, as recommended by *Yang et al.* [2004], geometric averages of all input quantities were used for the calculation of Φ and XO_2 mixing ratios to minimize the possibility of bias caused by measurement imprecision. Data were excluded from our analysis when the boat was moving or when pollution from the diesel generator was present. About 43% of the remaining number of data points was below the detection limit for NO (6% for NO_2). These data were not eliminated from the time series but are treated with caution for the PSS calculations (see below).

[16] The PSS approach should not be applied under "non–steady state" conditions, that is, when rapid changes of light intensity or mixing ratios occur. In order to exclude these cases, we calculated the time required to establish the PSS, τ_{PSS} (1/e-definition), according to

$$\tau_{PSS} = \frac{1}{j(\mathrm{NO_2}) + k_3 \times [\mathrm{O_3}]} \tag{2}$$

[17] The calculated τ_{PSS} values ranged between 60 and 300 s during daytime. When analyzing the 1 min time series, we found that trace gas mixing ratios typically remained fairly constant within these short time periods. Similar to previous studies [e.g., *Yang et al.*, 2004], we ensured adequate stability of $j(NO_2)$ by excluding data from the PSS evaluation during periods when the standard deviation of the solar global irradiance of the 10 min averaging interval was higher than 5% of the average value. Since radiation strongly varies during sunrise and sunset, these periods were automatically removed from the PSS evaluation based on this criterion. Thus, our analysis is confined to clear-sky periods with low radiation fluctuations (see below).

[18] Moreover, we estimated the prevailing XO_2 mixing ratios under "steady-state" conditions for cases when $\Phi > 1$, expressing their role in the conversion of NO to NO_2, by assuming that NO_2 is produced via reactions (R3), (R4), and (R5) and rearranging equation (1) as follows [*Carpenter et al.*, 1998; *Volz-Thomas et al.*, 2003]:

$$[\mathrm{XO_2}] = \sum_i [\mathrm{R}_i\mathrm{O_2}] + [\mathrm{HO_2}] = (\Phi - 1)\frac{k_3[\mathrm{O_3}]}{k_{eff}} \tag{3}$$

[19] Since the rate constants k_4 and k_5 are nearly identical [*Atkinson et al.*, 2004, 2006], we used an effective rate constant $k_4 \approx k_5 = k_{eff} = 3.6 \times 10^{-12} \exp(270/T)$ cm^3 $molecule^{-1}$ s^{-1} for

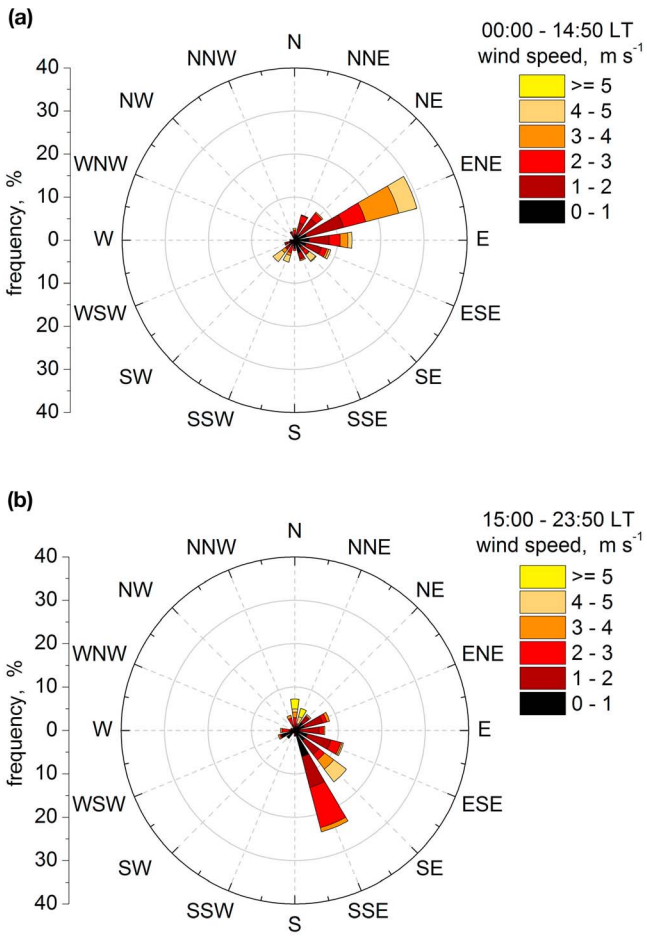

Figure 2. Wind roses for (a) 00:00 to 14:50 LT and (b) 15:00 to 23:50 LT including 10 min averaged wind data from all locations shown in Figure 1 except 26/27 July (for explanation see text) during the LBA-CLAIRE-2001 boat experiment. The time periods chosen for the wind roses are in accordance with the study by *de Oliveira and Fitzjarrald* [1993].

our analysis. It should be noted that equation (3) only holds in case no other processes convert NO to NO_2 (i.e., it ignores the potential role of NO_3 and halogens).

2.6. Measurement Uncertainties

[20] Photolytic converters which emit radiation in a very narrow spectral band, making the conversion of NO_2 to NO more specific (e.g., blue-light converters) were unfortunately not yet available in 2001. However, the high-pressure xenon lamp of the Tecan PLC 760 photolytic converter was equipped with an optical filter with a maximal transmittance at 360 nm. As discussed in the study by *Ryerson et al.* [2000], this minimizes interferences from other species (e.g., HONO). Under clean conditions, the HONO mixing ratio is about 50 ppt during daytime in the Amazon Basin [*Trebs et al.*, 2004]. The residence time of the air in the converter was 8 s (52% conversion efficiency) and with $j(\mathrm{HONO}) = 0.3 \times j(\mathrm{NO_2})$, the potential maximal HONO interference is thus approximately 8 ppt. The thermal decomposition of peroxyacetylnitrate (PAN) at 30°C for a residence time of 8 s is <1%. Assuming an upper limit of 500 ppt, the maximal PAN interference would be ~3 ppt. In addition, the zero-air measurement (see section 2.3) revealed no indication for a spurious NO_2 signal induced by irradiation of photolysis cell surfaces as described in the study by *Kley and McFarland* [1980]. The light stream in the photolysis cell was focused in a long narrow cylinder, thereby minimizing irradiation of the chamber walls that may cause secondary reactions.

[21] The uncertainty of the Leighton ratio can be estimated using Gaussian error propagation [cf. *Hauglustaine et al.*, 1996; *Mannschreck et al.*, 2004] (general formulation, see *Taylor* [1997]). An uncertainty of 20% was assigned to the rate constant k_3 [see *Atkinson et al.*, 2004]. Since we did not measure $j(\mathrm{NO_2})$, we applied an empirical parameterization (derived from in situ measurements in the Amazon) from *Trebs et al.* [2009] to estimate $j(\mathrm{NO_2})$ from the measured solar global irradiance. This method has a 2σ uncertainty of about 25%. An error of 5% was assigned to the ozone mixing ratio. The uncertainty of the NO and NO_2 measurements was estimated from the statistical error and the systematic error [cf. *Yang et al.*, 2004]. The statistical error (2σ-definition) comprises the detection limit (75 ppt for NO and 135 ppt for NO_2) and the analyzer precision of 4% (see section 2.3). The systematic error from calibrations and potential artifacts and uncertainties that could not be determined directly from our measurements (see above) was estimated to be 20%. The uncertainty increases with decreasing signal-to-noise ratio, and it was less than 30% for [NO] higher than 0.8 ppb and $[NO_2]$ higher than 1.4 ppb, 30%–95% for [NO] = 0.1–0.8 ppb and $[NO_2]$ = 0.2–1.4 ppb, and higher than 95% for [NO] less than 0.1 ppb and $[NO_2]$ less than 0.2 ppb. Hence, the estimated uncertainty of Φ (see section 3.4.2) is clearly dominated by the errors of the NO_x measurements, in particular, when mixing ratios approach the LOD. The uncertainty of estimated XO_2 mixing ratios was also estimated using Gaussian error propagation. Considering that mainly HO_2, CH_3O_2, and $C_2H_5O_2$ contribute to XO_2, an average uncertainty of 20% was assigned to the rate constant k_{eff} [see *Atkinson et al.*, 2004, 2006].

3. Results and Discussion

[22] Our data set includes 5 days of remote measurements when relatively clean air masses were sampled with only occasional anthropogenic influence, distinguishing three different cases (Figure 1). These are (1) 10–11 July (3.0324°S, 61.3445°W, "*Lago Manacapuru*," distance to Manaus ~147 km, color-code blue), (2) 18–19 July (3.0948°S, 60.4102°W, distance to Manaus ~43 km, color-code orange), and (3) 25 July (3.0316°S, 60.4736°W, distance to Manaus ~50 km, color-code turquoise). In addition, we observed two distinct cases when air masses were substantially influenced by anthropogenic pollution from the city of Manaus. These are (1) 20 July (3.0922°S, 60.1968°W, distance to Manaus ~19 km, color-code violet) and (2) 26–27 July (3.0185°S, 60.1725°W, distance to Manaus ~19 km, color-code magenta).

3.1. Meteorological Conditions

[23] The convective boundary layer (CBL) above the Amazonian rain forest typically reaches its maximum height

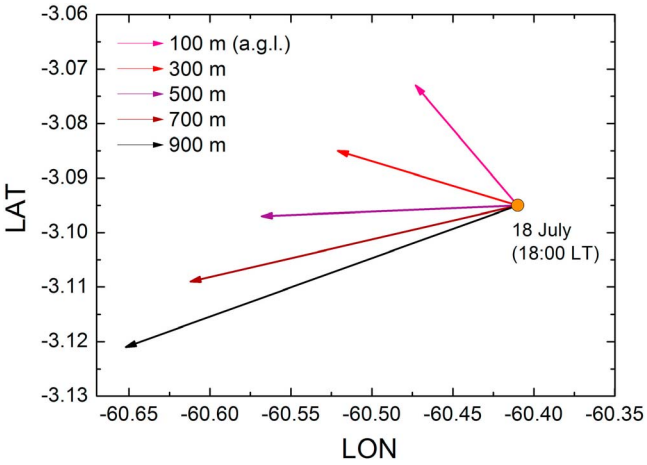

Figure 3. Wind vectors (expressed as 1 hour forward trajectories) calculated for five different heights within the CBL using the HYSPLIT model based on the meteorological REANALYSIS data set. The start time at the boat position on 18 July (3.0948°S, 60.4102°W) was 18:00 LT.

of 1000 to 1500 m at around 17:00 LT [*Fisch et al.*, 2004; *Martin et al.*, 1988]. Radiative cooling starts after 17:00 LT, and the thermodynamically stable stratified nocturnal boundary layer develops to a final height of 100 to 300 m. Meteorological conditions at the boat platform were mainly determined by background synoptic winds (northeasterly trade winds) and the formation of thermally driven diurnal mesoscale circulations. Wind roses averaged for all boat locations at the southern bank of the rivers (Figure 1) reveal prevailing winds from east-northeast during the night and morning (Figure 2a), while during the afternoon and evening, winds from south-southeast were dominating (Figure 2b). Both regimes are characterized by relatively high wind speeds (2 to 5 m s^{-1}). The transition between the two regimes typically occurred around 15:00 and 00:00 LT. A similar pattern had been observed previously by *Oliveira and Fitzjarrald* [1993] from measurements in an area north of the Rio Negro, about 60 km north of Manaus. They hypothesized that this circulation pattern can be attributed to a river breeze caused by the thermal contrast between the Rio Negro and the land surface. They found that the river breeze is asymmetric (i.e., not exactly perpendicular to the river) because of the influence of the easterly trade winds.

[24] This wind pattern was most distinct on 18/19 July. The Hybrid Single-Particle Lagrangian Integrated Trajectory (HYSPLIT) model [*Draxler and Hess*, 1998; meteorological REANALYSIS data set] provided supporting information on the dispersion of air masses originating from Manaus. Wind vectors expressed as 1 hour forward trajectories starting at 3.0948°S, 60.4102°W on 18 July at 18:00 LT at different heights within the CBL (Figure 3) reveal a southeasterly wind direction in the lower part of the boundary layer (<300 m), which agrees with our observations (Figure 4a). This was also experimentally confirmed by results of radio soundings at the K34 tower (not shown). The wind direction turned toward northeast with increasing height, indicating that the southeastern flow close to the ground was generated by processes within the CBL (e.g., decoupling, local pressure gradients). On 18/19 July, the wind direction measured on the boat platform also compares quite well with the wind direction measured at the K34 tower about 58 km north-northeast of the boat position (see Figure 4a). This confirms the existence of a mesoscale circulation system. *Betts et al.* [2009] pointed out that the generation of such mesoscale systems is not only caused by river breezes (depending on the shape of the rivers and their position toward the background synoptic flow) but may also be facilitated by other surface heterogeneities (topography, differences in roughness length between water and land, different vegetation types, and soil water availability). Results from the HYSPLIT model for days outside our measurement period indicate that this wind system is not always prevailing around the Manaus region, but was obviously the predominant pattern during the particular days when our measurements took place.

[25] We observed one significant exception from the typical wind pattern, which occurred on 26 and 27 July, the only instance when the boat was located at the northern bank of the Rio Negro close to Manaus (Figure 1). A diel oscillation of the local wind perpendicular to the river was observed. The wind blew from the rain forest (north) to the Rio Negro river during nighttime and from the river (south) to the rain forest during daytime (Figure 4a), which we attribute to a symmetrical river breeze.

[26] Typical daytime wind speeds measured on the boat were 2 to 5 m s^{-1}, and during nighttime the wind speed dropped to values between 0.5 and 2 m s^{-1} (Figure 4a). The RH typically ranged from 60% during daytime up to 90%–100% during nighttime (Figure 4b). Daytime and nighttime temperatures ranged between 29°C–32°C and 23°C–26°C, respectively. The global irradiance featured a typical diel course with maximal values of 900–1000 W m^{-2} during clear-sky periods (Figure 4c). On most days, cloudy skies prevailed during the afternoon hours when rain showers and, occasionally, thunderstorms occurred.

3.2. Trace Gas Mixing Ratios and Aerosol Concentrations

3.2.1. Ozone (O_3)

[27] The O_3 mixing ratios reveal a typical diel cycle with significantly higher values during daytime (Figure 4c). For the remote cases on 10, 18, and 19 July, a near twofold increase of the O_3 mixing ratios during the late afternoon indicates the influence of anthropogenic pollution (see below). Excluding these events, the measured daytime O_3 mixing ratios for the remote cases (10–11, 18–19, and 25 July) were on average 21 $\pm$ 2 ppb. For comparison, *Kuhn et al.* [2010] measured background O_3 mixing ratios of 18 to 24 ppb downwind of Manaus during the LBA-CLAIRE-2001 airborne measurements. Wet season median daytime O_3 values measured by *Rummel et al.* [2007] over a remote rain forest canopy were around 13 ppb, which is substantially lower than our values.

[28] Observed daytime O_3 mixing ratios for the polluted cases (20 and 26–27 July) were on average 31 $\pm$ 14 ppb with maximal values of 60 ppb on 26 July at a distance 19 km downwind of Manaus. *Kuhn et al.* [2010] observed maximal O_3 mixing ratios of 65 ppb at 100 km distance from Manaus in photochemically aged air masses at altitudes of several hundred meters above ground.

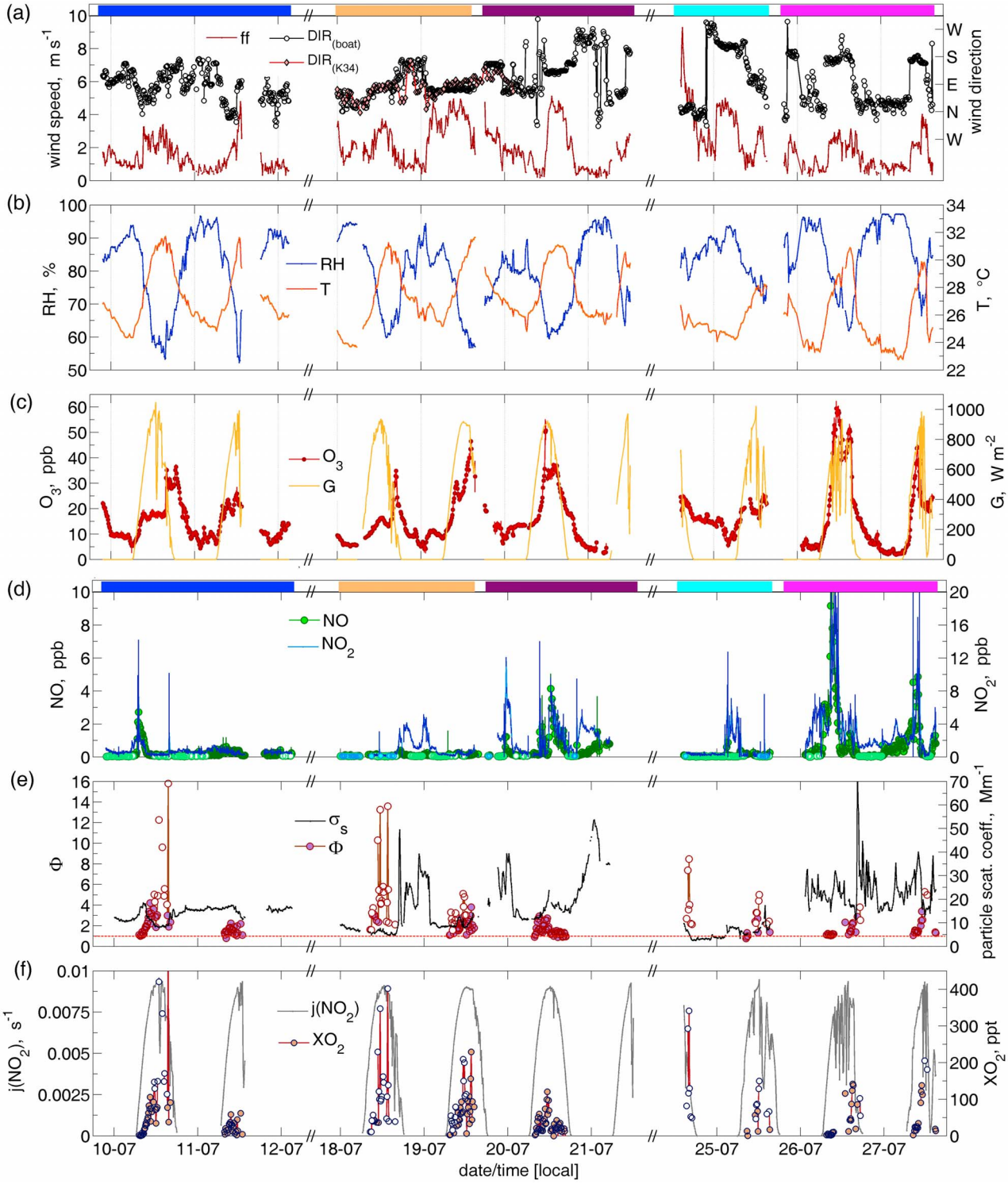

Figure 4. Measured and calculated time series (10 min averages) of (a) wind speed (ff) and wind direction (DIR, for 18/19 July also shown for the K34 tower site about 58 km NNE of the boat), (b) RH and air temperature (T), (c) global irradiance (G) and O_3 mixing ratios, (d) NO and NO_2 mixing ratio, (e) aerosol scattering coefficient (σ_s) and the Leighton ratio, ($\mathbf{\Phi}$), and (f) $j(NO_2)$ and the inferred XO_2 mixing ratio during 10–11, 18–20, and 25–27 July 2001 for the LBA-CLAIRE-2001 boat experiment. Error bars for trace gas measurements indicate standard deviations. Measured data points below the LOD and $\mathbf{\Phi}$ values and XO_2 mixing ratios calculated from NO or NO_2 mixing ratios below the LOD are represented by light or white circles. Gaps are caused by data rejection because of local contamination by moving boats or the diesel generator and the application of the steady-state criterion. The color code at the top refers to the locations of the boat platform shown in Figure 1.

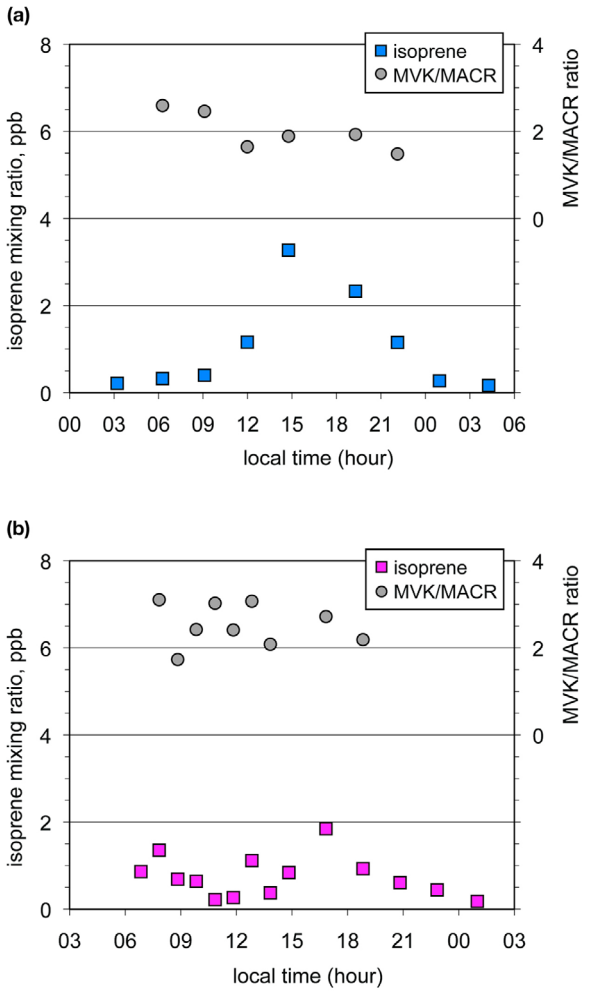

Figure 5. Measured isoprene mixing ratios and MVK/MACR ratios on (a) 10 July (remote case) and (b) 26 July (polluted case) during the LBA-CLAIRE-2001 boat experiment.

[29] Furthermore, we observed major differences in nighttime O_3 mixing ratios depending on whether or not the air had a riverine or a tropical forest footprint (Figures 1, 4a, and 4c). Nighttime O_3 mixing ratios were often considerably higher (~10 ppb) than measured above a tropical rain forest (<5 ppb) [see e.g., *Rummel et al.*, 2007]. This can be explained by: (1) the less stable nocturnal thermal stratification over (still warm) water surfaces than over land, facilitating intermittent downward transport of O_3 from aloft and (2) depending on the residence time of the air masses over the river, also by a smaller efficiency of O_3 uptake by a water surface than by vegetation [*Ganzeveld et al.*, 2009; *Wesely et al.*, 1981]. One exception was found during nighttime on 26/27 July (symmetric river breeze, see section 3.1), when air masses with O_3 well below 5 ppb were advected directly from the rain forest. Ozone dry deposition and removal through reaction with soil-biogenic NO emissions accumulated in the forest trunk space [*Rummel*, 2005] resulted in much lower nighttime O_3 levels than observed at the other locations.

3.2.2. Nitric Oxide (NO) and Nitrogen Dioxide (NO_2)

[30] The mixing ratios of NO for the remote cases on 10–11, 18–19, and 25 July were mostly lower than 500 ppt and sometimes fell below the detection limit of 75 ppt (Figure 4d). These values compare well with NO mixing ratios measured by *Bakwin et al.* [1990] and *Rummel* [2005] during the Amazonian wet season within and above the rain forest canopy. The major NO source under these remote conditions is biogenic emission from forest soils, potentially enhancing the NO_x mixing ratios of sub-canopy air masses being sampled at our measurement location on the river as a result of advection. Since the O_3 mixing ratios within and below the forest canopy are typically much lower than above the forest [see *Rummel et al.*, 2007], such events are mostly accompanied by a drop in the O_3 mixing ratio. Fresh pollution from biomass burning was sometimes transported to the boat (e.g., 10 July after 6:00 LT, see Figure 4d). On 19 and 20 July, the wind direction changed abruptly from south-southeast to east-northeast around midnight (see above), resulting in a NO mixing ratio increase to 0.6–1.0 ppb accompanied by a drop of the O_3 mixing ratio. The measured NO mixing ratios for the polluted cases (20 and 26–27 July) were largely influenced by fresh pollution originating from anthropogenic activities close to Manaus. During these events, NO mixing ratios reached values of up to 4–10 ppb before midday (Figure 4d).

[31] For the remote cases, the NO_2 mixing ratios were typically close to the detection limit of 135 ppt, for example, on 10 July around midday or on 25 July during nighttime (Figure 4d). Very low NO_2 mixing ratios (<300 ppt) were also observed on 18 July from 00:00 to 15:00 LT at a distance of ~43 km from Manaus on the Rio Negro. After that, the typical change of the wind direction from east-northeast to south-southeast (Figures 2 and 4a) resulted in an NO_2 increase to about 3 ppb while NO mixing ratios remained low, suggesting the arrival of an aged pollution plume (indicated also by an increase of O_3, see above) that lasted until the early morning of the next day. A similar event occurred on 19 July with even higher NO_2 mixing ratios.

[32] However, close to Manaus, on 26–27 July, NO_2 mixing ratios were typically highest before midday reaching a maximum of 18 ppb in the morning of 26 July. Comparably high NO_2 mixing ratios of about 16 ppb were also observed during the airborne measurements (410 m above ground level) on 15 July during the same time at nearly the same distance west of Manaus and were attributed to the plume originating from power plants in the southern part of the city [*Kuhn et al.*, 2010].

3.2.3. VOCs

[33] VOC mixing ratios and MVK/MACR ratios are presented for a remote (background) case (10 July, distance to Manaus ~147 km) and for a polluted case close to Manaus (26 July, distance to Manaus ~19 km) (see Figures 5a and 5b). As described in detail by *Kuhn et al.* [2007, 2010], for tower-based and airborne measurements during LBA-CLAIRE-2001, isoprene was the dominant compound observed, followed by the monoterpene α-pinene, both being emitted in a light-dependent manner [see *Kuhn et al.*, 2004]. While for the remote case, a typical diel pattern for biogenic isoprene with daytime maxima of about 3 ppb was observed (Figure 5a), the polluted case revealed somewhat lower mixing ratios during daytime (<2 ppb, Figure 5b), which was at least partly caused by lower radiation (Figure 4c). The contribution of anthropogenic isoprene

emissions related to industrial activities and in particular to vehicle exhaust [*Borbon et al.*, 2001; *Duane et al.*, 2002; *Reimann et al.*, 2000] might be a reasonable explanation for the higher variability for the polluted case, particularly during nighttime. The diel cycle of α-pinene resembles that of isoprene with maximal daytime mixing ratios of 0.2 ppb (not shown).

[34] The isoprene degradation reactions yield the unsaturated C4 carbonyls MACR and MVK plus formaldehyde (HCHO). High concentrations of these carbonyls as well as formaldehyde have been found previously in the tropical atmosphere [*Kesselmeier et al.*, 2002]. They constituted a significant fraction of VOC in the remote background case as well as in the polluted case close to Manaus during LBA-CLAIRE-2001 [*Kuhn et al.*, 2010]. The observed MVK/MACR values close to (and exceeding) a value of 2 resemble those measured throughout the CBL during LBA-CLAIRE-2001 [*Kuhn et al.*, 2010] and are indicative of OH-dominated isoprene degradation [see *Kuhn et al.*, 2007, 2010], where OH adds to one of the double bonds of isoprene, forming alkyl radicals that in turn add O_2 to form peroxy radicals (RO_2).

3.2.4. Aerosol Scattering Coefficient

[35] For the remote cases, the lowest values of the aerosol scattering coefficient (σ_s) ranged from 3 to 10 Mm^{-1} during daytime (Figure 4e). These values are comparable to the background airborne measurements in the boundary layer made during LBA-CLAIRE-2001 by *Kuhn et al.* [2010], as well as to those measured by *Guyon et al.* [2003] in southern Amazonia during the wet season. Nighttime σ_s values were typically several times higher, which was most likely also related to the change of the wind direction in the late afternoon (particularly evident on 18/19 July) and the influence of a pollution plume, as already found for O_3 and NO_2. Maximal σ_s values were 50–60 Mm^{-1} for the polluted cases.

[36] As shown in the previous sections, the remote cases were occasionally influenced by anthropogenic pollution during the afternoon. For further analysis, we classify our data in remote and polluted cases according to the prevailing σ_s, which constitutes a quantity that is relatively independent of the trace gas mixing ratios. *Guyon et al.* [2003] found that σ_s values representative for pristine background conditions are typically below 11 Mm^{-1}. In our case, this corresponds to NO_x mixing ratios below approximately 0.6 ppb. Henceforth, we refer to remote cases (mainly clean air masses with very minor influence of anthropogenic pollution) with $\sigma_s < 11$ Mm^{-1} and $NO_x < 0.6$ ppb and to polluted cases with $\sigma_s > 11$ Mm^{-1} and $NO_x > 0.6$ ppb.

3.3. Impact of the Manaus Plume

[37] The impact of the Manaus plume on Amazonian remote background conditions can be studied very well on 10, 18, and 19 July. During all three days, we measured a near twofold increase of the O_3 mixing ratio in the late afternoon (see section 3.2.1), which was caused by the typical change of the wind direction from east-northeast to south-southeast. On 10 July (distance to Manaus ~147 km), after 15:40 LT, the O_3 mixing ratio increased sharply from 19 to 32 ppb within a few minutes (Figure 4c). Besides the potential impact of anthropogenic pollution, a sudden drop in global irradiance indicates an increase in cloud cover associated with a thunderstorm, which occurred near the boat location. According to the study by *Betts et al.* [2002], this O_3 increase may suggest the occurrence of a strong convective downdraft, which brought O_3-rich air from the lower troposphere down to the surface. However, results from the HYSPLIT model indicate that the boat was located north of the Manaus plume in the morning, but caused by a change of the wind direction to south-southeast near the surface, the plume swung northward in the afternoon and reached the boat location at around 16:00 LT (not shown).

[38] We demonstrate this pattern in further detail for 18 and 19 July (distance to Manaus ~43 km), when comparable increases of the O_3 mixing ratio were observed. Figure 6 shows results of air mass dispersion calculations with the HYSPLIT model for 18 July. The main flow was from northeast before midday, and the plume did not reach the boat (Figure 6a). Measured trace gas mixing ratios and aerosol concentrations around midday were close to Amazonian background conditions ([NO] ~ 50 ppt (<LOD), $[NO_2]$ = 200 ppt, $[O_3]$ = 16 ppb, and σ_s = 6 Mm^{-1}) (Figure 4). The change of the wind direction to south-southeast near the surface in the late afternoon (measured on the boat and calculated from HYSPLIT, see Figures 2 and 4) is evident in Figure 6b, causing a northward swing of the plume that now reached the boat. Accordingly, trace gas mixing ratios and aerosol concentrations increased substantially ([NO] = 300 ppt, $[NO_2]$ = 3 ppb, $[O_3]$ = 35 ppb, and σ_s = 30 Mm^{-1}).

[39] Since no airborne measurements west of Manaus were made on 18 July, we further validate these findings using results from Flight 18: 10:00–14:00 LT and Flight 19: 15:45–18:00 LT on 19 July [see *Kuhn et al.*, 2010]. This can be justified by the fact that (1) the diel cycle of the wind direction is nearly identical for 18 and 19 July (Figure 4a), (2) the diel variation of O_3 mixing ratios shows a comparable pattern for 18 and 19 July (Figure 4c), and (3) in agreement with our wind measurements at the boat and at the K34 tower site (see above, Figure 4a) the HYSPLIT dispersion calculations reveal a comparable result for 18 and 19 July. After takeoff from Manaus airport, Flights 18 and 19 were set up as a Lagrangian experiment with a series of stacked horizontal profiles [*Kuhn et al.*, 2010]. We use results measured at various altitudes for a longitude of ~60.41°W directly over the boat. On 19 July, between 11:08 LT and 11:40 LT, the O_3 mixing ratios were 26, 28, 29, 23, and 33 ppb at heights of 3 m (boat), 30, 220, 544, and 860 m above ground level, respectively. These vertical mixing ratio differences suggest that convective transport away from the surface enables precursor compounds to achieve their full ozone generating potential [cf. *Kuhn et al.*, 2010].

[40] Figure 7 presents crosswind transects in the urban outflow for O_3 and CN concentrations at 220 m above ground level. Just before midday (11:25–11:34 LT, Flight 18), on 19 July, the boat was located at the northern edge of the plume (3.0948°S, 60.4102°W) (Figure 7). Compared to 18 July, when no anthropogenic influence was present just before midday, O_3 mixing ratios measured on the boat were slightly elevated (26 ppb) at 11:31 LT (the time the airplane flew over) on 19 July. In the afternoon, the O_3 mixing ratio on the boat was 30 ppb when the airplane flew over again at 16:45, while a mixing ratio of 34 ppb was measured at a height of 220 m above ground level (Figure 7). The center of the plume before midday ($[O_3]$ = 44 ppb) was at around

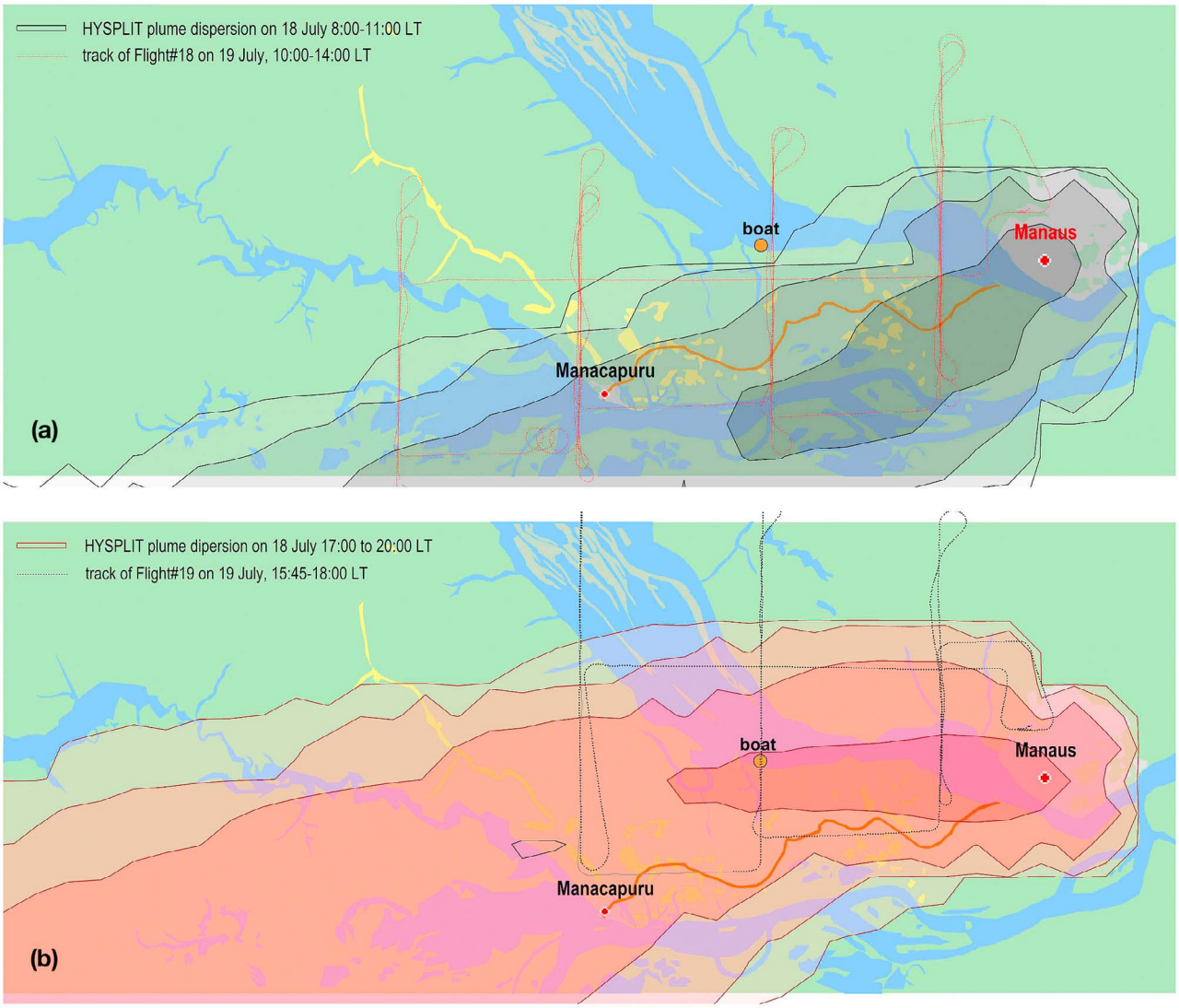

Figure 6. Simplified GIS map showing the study area during the LBA-CLAIRE-2001 boat experiment (orange circle shows the boat location on 18/19 July) including the results of a HYSPLIT dispersion model run (0–1000 m level) based on the meteorological REANALYSIS data set. The start time in Manaus City (3.11°S, 60.03°W) was at 08:00 LT on 17 July. The duration of the run was 36 hours. Shown are average air mass dispersions for (a) 18 July, 08:00–11:00 LT indicated by the gray contours and (b) 18 July, 17:00 to 20:00 LT indicated by the red contours. The flight tracks of Flight 18: 10:00–14:00 LT (Figure 6a) and Flight 19: 15:45–18:00 LT (Figure 6b) on 19 July are also shown.

3.18°S (south of the Rio Negro); while during the afternoon (16:40–16:48 LT, Flight 19), the center ($[O_3]$ = 50 ppb) was at around 3°S (northern bank of the Rio Negro). This is also visible in the corresponding CN concentrations. Hence, Figure 7 strongly suggests that the plume indeed swung northward as already indicated by results from the HYSPLIT model because of the southeasterly flow component (Figures 3 and 6). Apparently, the center of the plume swept over the boat platform around 14:00 LT, when O_3 mixing ratios on the boat exceeded 40 ppb. Hence, we sampled air masses that were significantly affected by anthropogenic pollution from Manaus during the afternoon. The arrival of the plume at the boat platform on 18/19 July is also evident from NO_2 mixing ratios and σ_s values that increased substantially during the late afternoon and typically remained high during the whole night. On 20 July, elevated mixing ratios measured on the boat in the proximity of Manaus (~19 km distance) suggest that the air masses sampled were influenced by the Manaus plume, which is supported by the results from the airborne measurements in the afternoon.

3.4. PSS

[41] As data measured during the afternoon often had to be rejected because of cloudy conditions (section 2.5, Figure 4c), only a limited number of data points was available for the PSS analysis. The application of the rejection criteria generally resulted in the rejection of measured NO_2 mixing ratios lower than NO_2 mixing ratios predicted by the PSS approach ($\Phi < 1$). Such cases might be attributed to local fresh NO emissions [cf. *Rohrer et al.*, 1998], for

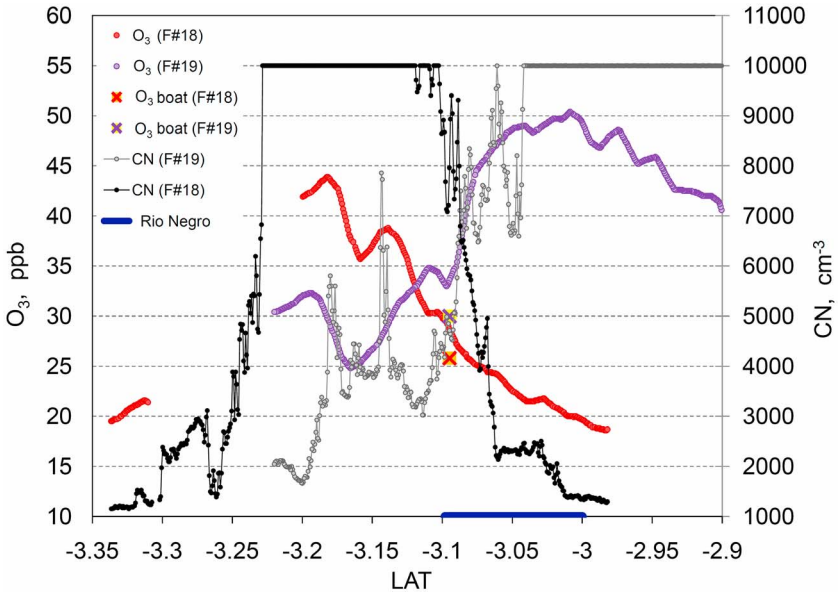

Figure 7. Measured O_3 mixing ratios and aerosol number (CN) concentrations (σ_s data were not always available) from crosswind transects in the urban outflow during Flight 18 and Flight 19 (10:00–14:00 and 15:45–18:00 LT on 19 July). Transects are shown for a longitude of approximately 60.41°W (~ 43 km downwind of Manaus) directly over the boat platform at 220 m (above ground level). CN data were cutoff at 10,000 cm^{-3} [cf. *Kuhn et al.*, 2010]. Corresponding O_3 mixing ratios measured at the boat platform when the airplane flew over (at 11:31 and 16:45 LT) are also shown.

example, from the generator and also to sunrise and sunset periods. Only 42% of the original daytime data could be used for the calculation of **Φ**. As shown in Figure 4e, the calculated **Φ** values (equation (1)) exceed unity in most cases. Just after sunrise (high solar zenith angle), **Φ** frequently reveals a tendency toward unity, which most likely is caused by the absence of peroxy radicals during this period. This is expected because during these times the emission of hydrocarbons from vegetation [e.g., *Kesselmeier and Staudt*, 1999] (see Figure 5) as well as photochemistry forming OH and peroxy radicals is still low [see *Griffin et al.*, 2007], and no significant additional oxidation pathway is present for NO. The deviation of **Φ** from unity sometimes follows the diel course of $j(NO_2)$ (Figure 4f), indicating the relationship to photochemically derived radicals, which is consistent with findings by, for example, *Griffin et al.* [2007] and *Rohrer et al.* [1998].

[42] We found the largest deviations from PSS (**Φ** > 2.5) for the clean remote cases (σ_s < 11 Mm^{-1} and NO_x < 0.6 ppb). This was mainly caused by the coincidence of NO mixing ratios below 200 ppt and low O_3 mixing ratios (13–17 ppb). For comparison, above a very remote Taiga woodland, *Bakwin et al.* [1994] found **Φ** values > 5, with prevailing NO_x levels <100 ppt and O_3 > 30 ppb. *Hauglustaine et al.* [1996] and *Ridley et al.* [1992] investigated PSS at the Mauna Loa Observatory in Hawaii, and despite remarkably low NO_x levels (<100 ppt), **Φ** values were less than 3. The significantly lower O_3 mixing ratios observed for our remote cases compared to the O_3 mixing ratios measured at Mauna Loa, coinciding with low NO mixing ratios, explain that our **Φ** values sometimes exceeded a value of 3. *Hosaynali Beygi et al.* [2011] found **Φ** values greater than 10 under pristine background conditions (NO_x = 5–25 ppt) in the Southern Atlantic boundary layer at O_3 levels of about 20 ppb.

[43] Previously reported near-ground **Φ** values at locations influenced by urban or suburban air masses were 1–3 [e.g., *Carpenter et al.*, 1998; *Griffin et al.*, 2007; *Matsumoto et al.*, 2006; *Parrish et al.*, 1986; *Rohrer et al.*, 1998; *Volz-Thomas et al.*, 2003]. These **Φ** values compare well with cases that were influenced by anthropogenic pollution in our study.

3.4.1. Influence of Environmental Factors and Anthropogenic Pollution on PSS

[44] Generally, the photochemical equilibrium is not reached, and **Φ** values deviate from unity when the timescales of turbulent transport are comparable or shorter than τ_{PSS}, for example, when there are nearby soil biogenic NO emissions and/or dry deposition of NO_2 and O_3. Turbulent timescales above a flat surface are often faster than the establishment of PSS (1–10 s) [cf. *Trebs et al.*, 2006], indicating that the photochemical equilibrium (steady state) may not be reached. Moreover, advection of O_3-depleted and NO_x-enriched air masses from the rain forest, reflecting an efficient dry deposition and reaction of O_3 with biogenic soil NO emissions in the trunk space, may have a significant influence on **Φ** values. However, these influences can be largely neglected if the footprint of the measurements consists of a fetch of open water, lacking substantial sources or sinks (deposition) of NO_x and O_3 (see section 3.2.1).

[45] Maximal **Φ** values were calculated for the clean remote cases (σ_s < 11 Mm^{-1}, NO_x < 0.6 ppb, mostly on 10, 18/19, and 24/25 July), comprising about 45% of all calculated **Φ** values. They ranged from 2.5 to 16, and the upper values were often derived from either NO or NO_2 mixing

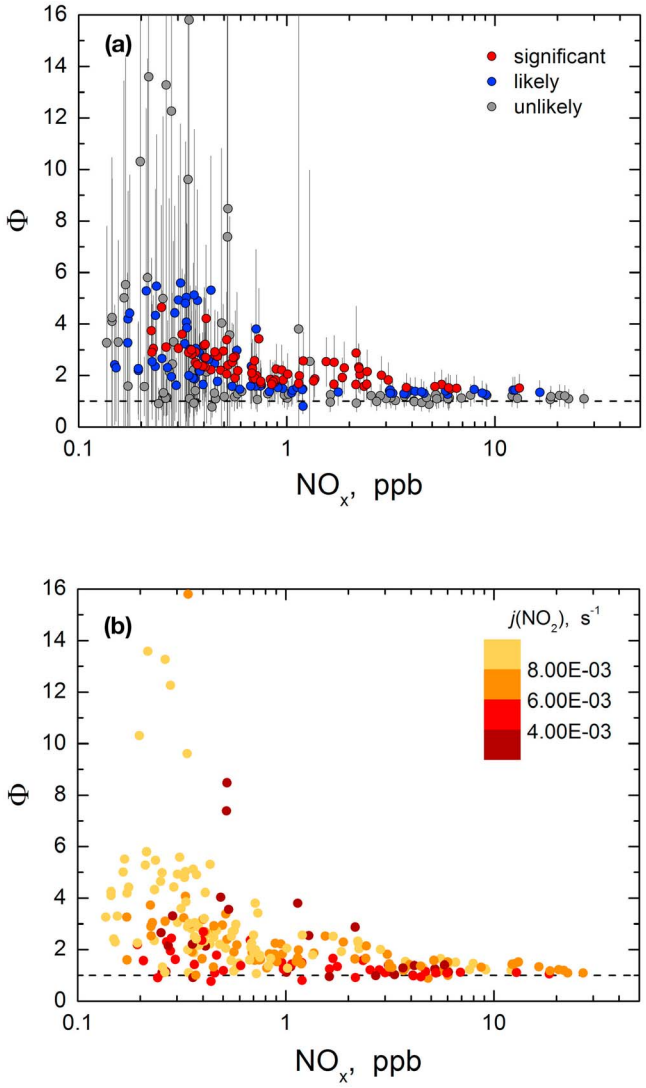

Figure 8. Leighton ratio, Φ, versus measured NO_x mixing ratios (geometric averages) from 10 to 11, 18–20, and 25–27 July 2001 (N = 239) (a) color-coded according to results from the statistical t test showing the Φ values that are significantly, likely and unlikely to be different from unity (for explanation, see text); error bars indicate the calculated uncertainty of Φ (2σ-definition) and (b) color-coded with $j(NO_2)$ during the LBA-CLAIRE-2001 boat experiment.

ratios below the LOD (white circles, Figure 4e). About 55% of the Φ values are assigned to polluted cases and were mostly below 2.

[46] Periods in the afternoon when a change of the wind direction occurred (see section 3.1) often coincided with periods of increased cloudiness because of convection (Figures 4a and 4c). Since the rejection criteria had to be applied during these periods (see above), an analysis of the influence of the Manaus plume arrival during 18/19 July (see section 3.3) on the diel evolution of Φ values was not possible. These periods also do not meet the steady-state criterion because of strong mixing ratio fluctuations (see e.g., 18 July, Figure 4c).

[47] However, we found that the Φ values were dependent on the position of the boat relative to the Manaus plume, and consequently, also on the distance of the measurement location to Manaus. From 18 to 20 July, we observed a gradual decline of calculated midday Φ values (Figure 4e). As previously shown, on 18 July no anthropogenic influence was present during midday, while on 19 July the boat was located at the edge of the plume, and on 20 July, the boat moved closer to Manaus, and the sampled air masses were strongly affected by the plume. The Φ values were closest to unity when polluted air was sampled, particularly on 20 and 26/27 July, when the distance of the boat was only 19 km from Manaus.

3.4.2. Discussion of Uncertainties and Dependence on NO_x

[48] Figure 8 combines the results from all locations. The uncertainty of Φ (error bars, 2σ-definition, see section 2.6) increases with decreasing NO_x. We used the one-sample t test [*Taylor*, 1997] to check if the calculated Φ values are unlikely (probability (p) < 95%), likely (95% ≤ p < 99%), or significantly (p ≥ 99%) different from unity (see Figure 8a). The results reveal that for NO_x < 3 ppb, 38% of the Φ values are significantly different from unity, 32% are likely, and only 30% are unlikely to be different from unity. Most of the high Φ values that are unlikely different from unity were calculated from NO or NO_2 mixing ratios below the LOD (see Figure 4e). The deviation of Φ from unity is most pronounced at NO_x mixing ratios below 1 ppb, whereas Φ approaches unity with increasing NO_x mixing ratios, which is the behavior also found in previous studies [e.g., *Griffin et al.*, 2007; *Volz-Thomas et al.*, 2003]. This trend is corroborated by the increase of Φ during midday (higher $j(NO_2)$ values, see Figure 8b), which is related to radical formation, as previously discussed. The Φ values close to unity at low NO_x mixing ratios are mainly confined to periods with lower $j(NO_2)$ and low VOC mixing ratios (see Figure 5) just after sunrise and before sunset. On the other hand, higher NO_x levels favor the rapid establishment of the PSS, as the sink for XO_2 increases when higher NO mixing ratios are present [cf. *Volz-Thomas et al.*, 2003]. Furthermore, under high-NO_x conditions the reaction of NO_2 with OH, forming HNO_3, leads to a competition with the oxidation of CO and hydrocarbons by OH, limiting the production of significant levels of peroxy radicals [e.g., *Mannschreck et al.*, 2004; *Volz-Thomas et al.*, 2003]. In our study, the ratio Φ reaches unity within its uncertainty range at NO_x mixing ratios of about 3 ppb. This value is comparable to studies at other locations and implies that no significant net production of ozone takes place at NO_x mixing ratios ≫ 3 ppb (corresponding to NO mixing ratios ≫ 1.4 ppb). For example, *Griffin et al.* [2007] also found Φ ∼ 1 at NO_x mixing ratios > 3 ppb and *Volz-Thomas et al.* [2003] found Φ ∼ 1 at NO mixing ratios > 1 ppb.

3.5. XO_2 Mixing Ratios

[49] The formation and cycling of radicals in tropical environments like the Amazon Basin is still subject of ongoing discussion. The high isoprene mixing ratios over tropical forest clearly have a considerably smaller effect on OH (depletion) than previously thought. Recent estimates and measurements within the CBL indicate that prevailing

Table 1. Comparison of XO_2 Mixing Ratios Modeled With CAABA/MECCA-3.0 to Those Derived From PSS (Equation (3)) for 10 July (Remote Case) and 26 July (Polluted Case)[a]

VOC Sample (Local Time)	XO_2 (Scenario 1[b]) (ppt)	XO_2 (Scenario 2[b]) (ppt)	Mean XO_2 (PSS) (ppt)
10 Jul 8:41–9:31	30	22	30
10 Jul 11:31–12:27	83	115	97
10 Jul 14:21–15:11	115	247	144
26 Jul 13:25–14:15	20	11	34
26 Jul 14:25–15:15	48	30	107
26 Jul 16:25–17:15	38	112	81

[a]The input values used for the model (NO, NO_2, O_3, H_2O, photolysis frequencies[b]) were averaged for the respective VOC sampling period. Mixing ratios of long-lived trace gases were kept constant (10 July: [CO] = 80 ppb, [CH_4] = 1820 ppb, 26 July: [CO] = 175 ppb, [CH_4] = 1875 ppb). Photolysis frequencies, such as $j(O(^1D))$, were calculated using the radiative transfer model Tropospheric Ultraviolet and Visible (TUV) v4.1. The ozone column was determined from Global Ozone Monitoring Experiment satellite data. The calculated photolysis frequencies were corrected for cloud and aerosol effects by scaling to $j(NO_2)$ [cf. *Kubistin et al.*, 2010].

[b]For explanation of scenarios see text.

OH concentrations are an order of magnitude higher (about 6×10^6 molecules cm^{-3} or 0.25 ppt, respectively) than currently predicted by state-of-the-art atmospheric chemistry models [see *Kuhn et al.*, 2007; *Ganzeveld et al.*, 2008; *Lelieveld et al.*, 2008; *Martinez et al.*, 2010; *Kubistin et al.*, 2010]. The presence of OH radicals controls the formation of XO_2 in the atmosphere through the oxidation of CO and hydrocarbons.

3.5.1. Estimation of XO_2 From PSS

[50] In this study, we provide estimates of XO_2 in the region west of Manaus according to equation (3) (see Figure 4f). It should be noted that some XO_2 mixing ratios were derived from either NO or NO_2 mixing ratios below the LOD (white circles, Figure 4f). Median midday/afternoon (PSS derived) XO_2 mixing ratios (equation (3)) for the remote cases ($\sigma_s < 11$ Mm^{-1} and $NO_x < 0.6$ ppb) range from 90 to 120 ppt, while for the polluted cases ($\sigma_s > 11$ Mm^{-1} and $NO_x > 0.6$ ppb) our estimates range from 15 to 60 ppt. The uncertainty of the peroxy radical mixing ratios is a function of Φ (see equation (3)) and often significantly exceeds 100%, which is mainly caused by the imprecision of the NO_x measurements at low mixing ratios (see section 2.6). This constitutes a major disadvantage of the PSS method to estimate XO_2. Furthermore, PSS is known to generally overestimate XO_2 mixing ratios by a factor of 2 or higher, which is most likely attributable to yet unidentified or unaccounted-for NO_2 formation pathways [*Cantrell et al.*, 1997; *Volz-Thomas et al.*, 2003; *Hosaynali Beygi et al.*, 2011].

3.5.2. Estimation of XO_2 Using a Chemistry Box Model

[51] We have additionally used the atmospheric chemistry box model, namely, the Chemistry As A Box model Application-Module Efficiently Calculating the Chemistry of the Atmosphere (CAABA/MECCA)-3.0 [*Sander et al.*, 2011], which contains the Mainz Isoprene Mechanism 2 (MIM2) [*Taraborrelli et al.*, 2009] to predict XO_2 mixing ratios. The model runs were constrained by fixing the measured species (NO, NO_2, O_3, H_2O, C_5H_8, MVK, and MACR) to their observed values (scenario 1). *Peeters and Müller* [2010] and *Peeters et al.* [2009] proposed that unimolecular reactions of certain RO_2 radicals lead to additional OH formation. Since MECCA-3.0 does not include these new reactions yet, it currently significantly under-predicts OH and consequently also underpredicts HO_2 within the CBL in the Amazon [see *Kubistin et al.*, 2010]. As a consequence, we performed additional model runs based on the first scenario but by also fixing OH [*Kuhn et al.*, 2007; *Martinez et al.*, 2010], HCHO [*Kesselmeier et al.*, 2002], and H_2O_2 [*Quesada et al.*, 2001] to measured values (scenario 2). For all cases, the model was run until a steady state value of HO_2 was reached. The results presented in Table 1 indicate that the predicted XO_2 mixing ratios are mostly within the range of those estimated by the PSS method. For scenario 2, the XO_2 predicted by the model would be two times lower if the OH mixing ratio fixed in the model input is reduced by a factor of 2. The modeled XO_2 is sometimes higher than the PSS estimates in the afternoon, which might be caused by the missing RO_2 sink attributed to the not yet included OH formation mechanism proposed by *Peeters and Müller* [2010] and *Peeters et al.* [2009] in MIM2. In the early afternoon of 26 July (polluted case), the XO_2 mixing ratios estimated from PSS significantly exceed the model results.

3.5.3. Comparison to Previous Results From Tropical Environments

[52] Mixing ratios of HO_2 only (providing a lower limit on the XO_2 mixing ratios), measured in the CBL over pristine rain forest in Suriname during the GABRIEL campaign, showed maxima of about 70 ppt around noontime [*Martinez et al.*, 2010]. Within the surface layer west of Manaus, the HO_2 mixing ratio calculated with a single column chemistry-climate model (SCM) [*Ganzeveld et al.*, 2002], also being applied in another study of the Manaus city plume [*Kuhn et al.*, 2010], reached 50 ppt, with the CH_3O_2 mixing ratio as small as 3 ppt during midday. The XO_2 mixing ratios measured in a comparably remote tropical environment in the rain forest of Borneo ranged from 20 to 40 ppt around midday [*Pugh et al.*, 2010].

4. Conclusions

[53] We have measured mixing ratios of the trace gases NO, NO_2, O_3, and VOCs as well as the aerosol scattering coefficient, σ_s, in a previously unexplored environment using a boat platform cruising on rivers west of Manaus (Amazon Basin) on 10–11, 18–20, and 25–27 July 2001. To our knowledge, these are the first trace gas measurements made on rivers in the Amazon Basin, which are unique locations for studying atmospheric processes within the tropical boundary layer. The temporal and spatial dispersion of the Manaus plume had a significant influence on the measured mixing ratios at the different boat locations. The measured trace gas mixing ratios and calculated Φ values reflect the interaction between river breezes and/or mesoscale circulations, and the impact of synoptic winds transporting pollution from Manaus to pristine areas of the Amazonian rain forest. In particular, during our measurement period, the wind mainly blew from east-northeast during the night and in the morning (influence of easterly trade winds), while wind directions from south-southeast dominated during the afternoon and evening. The remote cases with very minor anthropogenic influence were characterized

by σ_s values below 11 Mm^{-1} and NO_x below 0.6 ppb, coinciding with midday O_3 mixing ratios often lower than 20 ppb. For these cases, significant deviations from the PSS in the NO-NO_2-O_3 triad were observed. The combination of low NO (<200 ppt) with low O_3 (<20 ppb) in the absence of anthropogenic pollution caused the Leighton ratio, Φ, sometimes to be higher than 3. The change of the wind direction to south-southeast in the afternoon facilitated a northward swing of the Manaus plume, which then often reached the boat. These polluted air masses were characterized by σ_s values of about 30 Mm^{-1}, NO_x mixing ratios between 2 and 4 ppb, and by O_3 mixing ratios of up to 35 ppb. For these polluted cases, the calculated Φ values were close to unity. Despite the large uncertainties associated with the PSS method, the estimated XO_2 mixing ratios are within the range of results from the box model CAABA/MECCA-3.0. The results from both methods suggest that the XO_2 mixing ratios are at least a factor of 2 higher in remote areas west of Manaus compared to locations influenced by the Manaus urban plume. This implies that anthropogenic pollution from Manaus significantly alters the chemical composition of the otherwise pristine Amazonian background air near the surface. This may in turn have a significant influence on surface-atmosphere exchange processes of reactive species. The limited knowledge of HO_2 and RO_2 mixing ratios in tropical regions like the Amazon Basin emphasizes the need for in situ measurements in the near future to improve our understanding of O_3 production pathways and the cycling of reactive nitrogen as well as of OH and XO_2 in clean and polluted air masses.

[54] We anticipate that because of the rapidly growing population of Manaus to more than 1.7 million human inhabitants meanwhile, and consequently, the rising pollution levels, the impact on atmospheric chemistry in the region west of Manaus is growing. It is recommended to establish long-term monitoring stations downwind of Manaus and to apply mesoscale models to investigate the influence of the Rio Negro river breeze on the dispersion of the Manaus urban plume.

[55] **Acknowledgments.** The data presented in this study were acquired within the framework of LBA. The project was funded by the Max Planck Society. It was additionally supported by the Fundação de Amparo à Pesquisa do Estado de São Paulo (FAPESP), the Brazilian Conselho Nacional de Desenvolvimento Científico e Tecnológica (CNPq) and the Instituto Nacional de Pesquisas da Amazônia (INPA). We gratefully acknowledge Paraiso D'Angelo and its owner J. D'Angelo, the captains, the crew and the electrician of the boats, as well as the staff from the MPIC workshop. We like to thank A. Camargo and M. Richardson for their support during the measurements and P. Stefani and A.C. de Araújo for providing the meteorological data from the K34 tower. We are indebted to A. Thielmann and the aircraft team for the airborne measurements. We thank G. Schebeske for analyzing the VOC samples, B. Mamtimin for generating the GIS map of the study area and J.-C. Mayer for helping create the graphs. We are grateful to E. Regelin, D. Kubistin, and H. Harder for their support with the box model CAABA/MECCA-3.0 and to H. Fischer for the discussion of the results. We credit the NOAA Air Resources Laboratory for making the HYSPLIT transport and dispersion model available.

References

Andreae, M. O., et al. (1988), Biomass burning emissions and associated haze layers over Amazonia, *J. Geophys. Res.*, *93*(D2), 1509–1527, doi:10.1029/JD093iD02p01509.

Atkinson, R., D. L. Baulch, R. A. Cox, J. N. Crowley, R. F. Hampson, R. G. Hynes, M. E. Jenkin, M. J. Rossi, and J. Troe (2004), Evaluated kinetic and photochemical data for atmospheric chemistry: Volume I – Gas phase reactions of O_x, HO_x, NO_x and SO_x species, *Atmos. Chem. Phys.*, *4*, 1461–1738, doi:10.5194/acp-4-1461-2004.

Atkinson, R., D. L. Baulch, R. A. Cox, J. N. Crowley, R. F. Hampson, R. G. Hynes, M. E. Jenkin, M. J. Rossi, and J. Troe (2006), Evaluated kinetic and photochemical data for atmospheric chemistry: Volume II – Gas phase reactions of organic species, *Atmos. Chem. Phys.*, *6*, 3625–4055, doi:10.5194/acp-6-3625-2006.

Bakwin, P. S., S. C. Wofsy, and S. M. Fan (1990), Measurements of reactive nitrogen-oxides (NO_y) within and above a tropical forest canopy in the wet season, *J. Geophys. Res.*, *95*(D10), 16,765–16,772, doi:10.1029/JD095iD10p16765.

Bakwin, P. S., et al. (1994), Reactive Nitrogen-Oxides and Ozone above a Taiga Woodland, *J. Geophys. Res.*, *99*(D1), 1927–1936, doi:10.1029/93JD02292.

Betts, A. K., L. V. Gatti, A. M. Cordova, M. Dias, and J. D. Fuentes (2002), Transport of ozone to the surface by convective downdrafts at night, *J. Geophys. Res.*, *107*(D20), 8046, doi:10.1029/2000JD000158.

Betts, A. K., G. Fisch, C. von Randow, M. A. F. Silva Dias, J. C. P. Cohen, R. da Silva, and D. R. Fitzjarrald (2009), The Amazonian boundary layer and mesoscale circulations, in *Amazonia and Global Change*, *Geophys. Monogr. Ser.*, vol. 186, edited by M. Keller et al., pp. 163–181, AGU, Washington, D. C., doi:10.1029/2008GM000725.

Borbon, A., H. Fontaine, M. Veillerot, N. Locoge, J. C. Galloo, and R. Guillermo (2001), An investigation into the traffic-related fraction of isoprene at an urban location, *Atmos. Environ.*, *35*, 3749–3760, doi:10.1016/S1352-2310(01)00170-4.

Cantrell, C. A., R. E. Shetter, J. G. Calvert, F. L. Eisele, E. Williams, K. Baumann, W. H. Brune, P. S. Stevens, and J. H. Mather (1997), Peroxy radicals from photostationary state deviations and steady state calculations during the Tropospheric OH Photochemistry Experiment at Idaho Hill, Colorado, 1993, *J. Geophys. Res.*, *102*(D5), 6369–6378, doi:10.1029/96JD01703.

Carpenter, L. J., K. C. Clemitshaw, R. A. Burgess, S. A. Penkett, J. N. Cape, and G. C. McFadyen (1998), Investigation and evaluation of the NO_x/O_3 photochemical steady state, *Atmos. Environ.*, *32*, 3353–3365, doi:10.1016/S1352-2310(97)00416-0.

Crutzen, P. J., and J. Lelieveld (2001), Human impacts on atmospheric chemistry, *Annu. Rev. Earth Planet. Sci.*, *29*, 17–45, doi:10.1146/annurev.earth.29.1.17.

Crutzen, P. J., A. C. Delany, J. Greenberg, P. Haagenson, L. Heidt, R. Lueb, W. Pollock, W. Seiler, A. Wartburg, and P. Zimmerman (1985), Tropospheric chemical-composition measurements in Brazil during the dry season, *J. Atmos. Chem.*, *2*, 233–256, doi:10.1007/BF00051075.

Draxler, R. R., and G. D. Hess (1998), An overview of the HYSPLIT 4 modelling system for trajectories, dispersion and deposition, *Aust. Meteorol. Mag.*, *47*, 295–308.

Duane, M., B. Poma, D. Rembges, C. Astorga, and B. R. Larsen (2002), Isoprene and its degradation products as strong ozone precursors in Insubria, northern Italy, *Atmos. Environ.*, *36*, 3867–3879, doi:10.1016/S1352-2310(02)00359-X.

Fisch, G., J. Tota, L. A. T. Machado, M. Dias, R. F. D. Lyra, C. A. Nobre, A. J. Dolman, and J. H. C. Gash (2004), The convective boundary layer over pasture and forest in Amazonia, *Theor. Appl. Climatol.*, *78*, 47–59.

Ganzeveld, L. N., J. Lelieveld, F. J. Dentener, A. C. Krol, and G. Roelofs (2002), Atmosphere-biosphere trace gas exchanges simulated with a single-column model, *J. Geophys. Res.*, *107*(D16), 4297, doi:10.1029/2001JD000684.

Ganzeveld, L., et al. (2008), Surface and boundary layer exchanges of volatile organic compounds, nitrogen oxides and ozone during the GABRIEL campaign, *Atmos. Chem. Phys.*, *8*, 6223–6243, doi:10.5194/acp-8-6223-2008.

Ganzeveld, L., D. Helmig, C. W. Fairall, J. Hare, and A. Pozzer (2009), Atmosphere-ocean ozone exchange: A global modeling study of biogeochemical, atmospheric, and waterside turbulence dependencies, *Global Biogeochem. Cycles*, *23*, GB4021, doi:10.1029/2008GB003301.

Ganzeveld, L., L. Bouwman, E. Stehfest, D. P. van Vuuren, B. Eickhout, and J. Lelieveld (2010), Impact of future land use and land cover changes on atmospheric chemistry-climate interactions, *J. Geophys. Res.*, *115*, D23301, doi:10.1029/2010JD014041.

Griffin, R. J., P. J. Beckman, R. W. Talbot, B. C. Sive, and R. K. Varner (2007), Deviations from ozone photostationary state during the International Consortium for Atmospheric Research on Transport and Transformation 2004 campaign: Use of measurements and photochemical modeling to assess potential causes, *J. Geophys. Res.*, *112*, D10S07, doi:10.1029/2006JD007604.

Gut, A., et al. (2002), Exchange fluxes of NO_2 and O_3 at soil and leaf surfaces in an Amazonian rain forest, *J. Geophys. Res.*, *107*(D20), 8060, doi:10.1029/2001JD000654.

Guyon, P., B. Graham, J. Beck, O. Boucher, E. Gerasopoulos, O. L. Mayol-Bracero, G. C. Roberts, P. Artaxo, and M. O. Andreae (2003), Physical properties and concentration of aerosol particles over the Amazon tropical forest during background and biomass burning conditions, *Atmos. Chem. Phys.*, *3*, 951–967, doi:10.5194/acp-3-951-2003.

Harriss, R. C., et al. (1988), The Amazon boundary layer experiment (ABLE-2A): Dry season 1985, *J. Geophys. Res.*, *93*(D2), 1351–1360, doi:10.1029/JD093iD02p01351.

Hauglustaine, D. A., S. Madronich, B. A. Ridley, J. G. Walega, C. A. Cantrell, R. E. Shetter, and G. Hubler (1996), Observed and model-calculated photostationary state at Mauna Loa observatory during MLOPEX 2, *J. Geophys. Res.*, *101*(D9), 14,681–14,696, doi:10.1029/95JD03612.

Hosaynali Beygi, Z., H. Fischer, H. D. Harder, M. Martinez, R. Sander, J. Williams, D. M. Brookes, P. S. Monks, and J. Lelieveld (2011), Oxidation photochemistry in the Southern Atlantic boundary layer: Unexpected deviations of photochemical steady state, *Atmos. Chem. Phys.*, *11*, 8497–8513, doi:10.5194/acp-11-8497-2011.

Jacob, D. J., and S. C. Wofsy (1990), Budgets of reactive nitrogen, hydrocarbons, and ozone over the Amazon forest during the wet season, *J. Geophys. Res.*, *95*(D10), 16,737–16,754, doi:10.1029/JD095iD10p16737.

Kesselmeier, J., and M. Staudt (1999), Biogenic volatile organic compounds (VOC): An overview on emission, physiology and ecology, *J. Atmos. Chem.*, *33*, 23–88, doi:10.1023/A:1006127516791.

Kesselmeier, J., et al. (2002), Concentrations and species composition of atmospheric volatile organic compounds (VOCs) as observed during the wet and dry season in Rondonia (Amazonia), *J. Geophys. Res.*, *107*(D20), 8053, doi:10.1029/2000JD000267.

Kley, D., and M. McFarland (1980), Chemiluminescence detector for NO and NO_2, *Atmos. Technol.*, *12*, 62–69.

Kubistin, D., et al. (2010), Hydroxyl radicals in the tropical troposphere over the Suriname rainforest: Comparison of measurements with the box model MECCA, *Atmos. Chem. Phys.*, *10*(19), 9705–9728.

Kuhn, U., S. Rottenberger, T. Biesenthal, A. Wolf, G. Schebeske, P. Ciccioli, E. Brancaleoni, M. Frattoni, T. M. Tavares, and J. Kesselmeier (2002), Isoprene and monoterpene emissions of Amazonian tree species during the wet season: Direct and indirect investigations on controlling environmental functions, *J. Geophys. Res.*, *107*(D20), 8071, doi:10.1029/2001JD000978.

Kuhn, U., S. Rottenberger, T. Biesenthal, A. Wolf, G. Schebeske, P. Ciccioli, and J. Kesselmeier (2004), Strong correlation between isoprene emission and gross photosynthetic capacity during leaf phenology of the tropical tree species Hymenaea courbaril with fundamental changes in volatile organic compounds emission composition during early leaf development, *Plant Cell Environ.*, *27*, 1469–1485, doi:10.1111/j.1365-3040.2004.01252.x.

Kuhn, U., et al. (2007), Isoprene and monoterpene fluxes from Central Amazonian rainforest inferred from tower-based and airborne measurements, and implications on the atmospheric chemistry and the local carbon budget, *Atmos. Chem. Phys.*, *7*, 2855–2879, doi:10.5194/acp-7-2855-2007.

Kuhn, U., et al. (2010), Impact of Manaus City on the Amazon Green Ocean atmosphere: Ozone production, precursor sensitivity and aerosol load, *Atmos. Chem. Phys.*, *10*, 9251–9282, doi:10.5194/acp-10-9251-2010.

Leighton, P. A. (1961), *Photochemistry of Air Pollution*, Academic, San Diego, Calif.

Lelieveld, J., et al. (2008), Atmospheric oxidation capacity sustained by a tropical forest, *Nature*, *452*, 737–740, doi:10.1038/nature06870.

Mannschreck, K., S. Gilge, C. Plass-Duelmer, W. Fricke, and H. Berresheim (2004), Assessment of the applicability of $NO\text{-}NO_2\text{-}O_3$ photostationary state to long-term measurements at the Hohenpeissenberg GAW Station, Germany, *Atmos. Chem. Phys.*, *4*, 1265–1277, doi:10.5194/acp-4-1265-2004.

Martin, C. L., D. Fitzjarrald, M. Garstang, A. P. Oliveira, S. Greco, and E. Browell (1988), Structure and growth of the mixing layer over the Amazonian rain forest, *J. Geophys. Res.*, *93*(D2), 1361–1375, doi:10.1029/JD093iD02p01361.

Martinez, M., et al. (2010), Hydroxyl radicals in the tropical troposphere over the Suriname rainforest: Airborne measurements, *Atmos. Chem. Phys.*, *10*, 3759–3773, doi:10.5194/acp-10-3759-2010.

Matsumoto, J., N. Kosugi, A. Nishiyama, R. Isozaki, Y. Sadanaga, S. Kato, H. Bandow, and Y. Kajii (2006), Examination on photostationary state of NO_x in the urban atmosphere in Japan, *Atmos. Environ.*, *40*, 3230–3239, doi:10.1016/j.atmosenv.2006.02.002.

Oliveira, A. P., and D. R. Fitzjarrald (1993), The Amazon River breeze and the local boundary-layer: 1. Observations, *Boundary Layer Meteorol.*, *63*, 141–162, doi:10.1007/BF00705380.

Parrish, D. D., M. Trainer, E. J. Williams, D. W. Fahey, G. Hubler, C. S. Eubank, S. C. Liu, P. C. Murphy, D. L. Albritton, and F. C. Fehsenfeld (1986), Measurements of the $NO_x\text{-}O_3$ photostationary state at Niwot Ridge, Colorado, *J. Geophys. Res.*, *91*(D5), 5361–5370, doi:10.1029/JD091iD05p05361.

Peeters, J., and J.-F. Müller (2010), HO(x) radical regeneration in isoprene oxidation via peroxy radical isomerisations. II: Experimental evidence and global impact, *Phys. Chem. Chem. Phys.*, *12*, 14,227–14,235, doi:10.1039/c0cp00811g.

Peeters, J., T. L. Nguyen, and L. Vereecken (2009), HO_x radical regeneration in the oxidation of isoprene, *Phys. Chem. Chem. Phys.*, *11*, 5935–5939, doi:10.1039/b908511d.

Pugh, T. A. M., et al. (2010), Simulating atmospheric composition over a South-East Asian tropical rainforest: Performance of a chemistry box model, *Atmos. Chem. Phys.*, *10*, 279–298, doi:10.5194/acp-10-279-2010.

Quesada, J., D. Grossmann, E. Fernandez, J. Romero, E. Sanhueza, G. Moortgat, and P. J. Crutzen (2001), Ground based gas phase measurements in Surinam during the LBA-CLAIRE 98 experiment, *J. Atmos. Chem.*, *39*, 15–36, doi:10.1023/A:1010762209008.

Reimann, S., P. Calanca, and P. Hofer (2000), The anthropogenic contribution to isoprene concentrations in a rural atmosphere, *Atmos. Environ.*, *34*, 109–115, doi:10.1016/S1352-2310(99)00285-X.

Ridley, B. A., S. Madronich, R. B. Chatfield, J. G. Walega, R. E. Shetter, M. A. Carroll, and D. D. Montzka (1992), Measurements and model simulations of the photo stationary state during the Mauna-Loa-Observatory Photochemistry Experiment: Implications for radical concentrations and ozone production and loss rates, *J. Geophys. Res.*, *97*(D10), 10,375–10,388.

Rohrer, F., D. Bruning, E. S. Grobler, M. Weber, D. H. Ehhalt, R. Neubert, W. Schussler, and I. Levin (1998), Mixing ratios and photostationary state of NO and NO_2 observed during the POPCORN field campaign at a rural site in Germany, *J. Atmos. Chem.*, *31*, 119–137, doi:10.1023/A:1006166116242.

Rummel, U. (2005), *Turbulent Exchange of Ozone and Nitrogen Oxides Between an Amazonian Rain Forest and the Atmosphere*, Univ. of Bayreuth, Bayreuth, Germany.

Rummel, U., C. Ammann, A. Gut, F. X. Meixner, and M. O. Andreae (2002), Eddy covariance measurements of nitric oxide flux within an Amazonian rain forest, *J. Geophys. Res.*, *107*(D20), 8050, doi:10.1029/2001JD000520.

Rummel, U., C. Ammann, G. A. Kirkman, M. A. L. Moura, T. Foken, M. O. Andreae, and F. X. Meixner (2007), Seasonal variation of ozone deposition to a tropical rain forest in southwest Amazonia, *Atmos. Chem. Phys.*, *7*, 5415–5435, doi:10.5194/acp-7-5415-2007.

Ryerson, T. B., E. J. Williams, and F. C. Fehsenfeld (2000), An efficient photolysis system for fast-response NO_2 measurements, *J. Geophys. Res.*, *105*(D21), 26,447–26,461, doi:10.1029/2000JD900389.

Sander, R., et al. (2011), The atmospheric chemistry box model CAABA/MECCA-3.0, *Geosci. Model. Dev.*, *4*, 373–380, doi:10.5194/gmd-4-373-2011.

Taraborrelli, D., M. G. Lawrence, T. M. Butler, R. Sander, and J. Lelieveld (2009), Mainz Isoprene Mechanism 2(MIM2), An isoprene oxidation mechanism for regional and global atmospheric modelling, *Atmos. Chem. Phys.*, *9*, 2751–2777, doi:10.5194/acp-9-2751-2009.

Taylor, J. R. (1997), *An Introduction to Error Analysis: The Study of Uncertainties in Physical Measurements*, Univ. Sci. Books, Sausalito, Calif.

Torres, A. L., and H. Buchan (1988), Tropospheric nitric oxide measurements over the Amazon Basin, *J. Geophys. Res.*, *93*(D2), 1396–1406, doi:10.1029/JD093iD02p01396.

Trebs, I., F. X. Meixner, J. Slanina, R. P. Oties, P. Jongejan, and M. O. Andreae (2004), Real-time measurements of ammonia, acidic trace gases and water-soluble inorganic aerosol species at a rural site in the Amazon Basin, *Atmos. Chem. Phys.*, *4*, 967–987, doi:10.5194/acp-4-967-2004.

Trebs, I., L. S. Lara, L. M. Zeri, L. V. Gatti, P. Artaxo, R. Dlugi, J. Slanina, M. O. Andreae, and F. X. Meixner (2006), Dry and wet deposition of atmospheric inorganic nitrogen in a tropical environment (Rondônia, Brazil), *Atmos. Chem. Phys.*, *6*, 447–469, doi:10.5194/acp-6-447-2006.

Trebs, I., B. Bohn, C. Ammann, U. Rummel, M. Blumthaler, R. Königstedt, F. X. Meixner, S. Fan, and M. O. Andreae (2009), Relationship between the NO_2 photolysis frequency and the solar global irradiance, *Atmos. Meas. Tech.*, *2*, 725–739, doi:10.5194/amt-2-725-2009.

Volz-Thomas, A., H. W. Patz, N. Houben, S. Konrad, D. Mihelcic, T. Klupfel, and D. Perner (2003), Inorganic trace gases and peroxy radicals during BERLIOZ at Pabstthum: An investigation of the photostationary state of NO_x and O_3, *J. Geophys. Res.*, *108*(D4), 8248, doi:10.1029/2001JD001255.

Warneck, P. (2000), *Chemistry of the Natural Atmosphere* (2nd ed.), Academic, San Diego, Calif.

Wesely, M. L., D. R. Cook, and R. M. Williams (1981), Field measurement of small ozone fluxes to snow, wet bare soil, and lake water, *Boundary Layer Meteorol.*, *20*, 459–471, doi:10.1007/BF00122295.

Yang, J., R. E. Honrath, M. C. Peterson, D. D. Parrish, and M. Warshawsky (2004), Photostationary state deviation-estimated peroxy radicals and their implications for HO_x and ozone photochemistry at a remote northern Atlantic coastal site, *J. Geophys. Res.*, *109*, D02312, doi:10.1029/2003JD003983.

M. O. Andreae, J. Kesselmeier, F. X. Meixner, and I. Trebs, Biogeochemistry Department, Max Planck Institute for Chemistry, PO Box 3060, D-55020 Mainz, Germany. (i.trebs@mpic.de)

P. Artaxo, Instituto de Física, Universidade de São Paulo, Rua do Matão, Travessa R, 187, CEP 05508-900, São Paulo, SP, Brazil.

L. Ganzeveld, Department of Environmental Sciences, Wageningen University and Research Centre, Droevendaalsesteeg 4, NL-6708 PB Wageningen, Netherlands.

U. Kuhn, Institute of Energy and Climate Research: Troposphere, Juelich Research Center, D-52425 Juelich, Germany.

O. L. Mayol-Bracero, Institute for Tropical Ecosystem Studies, University of Puerto Rico, PO Box 70377, Río Piedras, PR 00936-8377.

T. Pauliquevis, Departamento de Ciências Exatas e da Terra, Universidade Federal de São Paulo, Rua Prof. Artur Riedel, 275, CEP 09972-270, Diadema, SP, Brazil.

R. Sander, Air Chemistry Department, Max Planck Institute for Chemistry, PO Box 3060, D-55020 Mainz, Germany.